J Nanostruct 11(3): 446-455, Summer 2021

RESEARCH PAPER

Nanostructured PEDOT: PSS /ZnO Heterojunction Diodes as Ultraviolet Sensors

Asrar Abdulmunem Saeed [1], *Abdullah Hussein* [2], *Tahseen Alaridhee* [2]* *and Fatima Malek* [2]

[1] *Department of physics, College of Science, Mustansiriyah University, 10052, Baghdad, Iraq*

[2] *Department of Material Science, Polymer Research Centre, University of Basrah, 61004, Basrah, Iraq*

ARTICLE INFO

Article History:
Received 03 May 2021
Accepted 24 June 2021
Published 01 July 2021

Keywords:
PEDOT: PSS
P-n junction
Radiation
UV sensor
ZnO NPs

ABSTRACT

Development in ultraviolet (UV) photodetectors get research community attention and incorporated in a wide range of applications. To improve light sensitivity, wideband gap nanotechnology was employed, such as zinc oxide for its notable properties. The vital role is on UV heterojunctibility sensing between ZnO NPs and polymer conducting nanocomposites (3, 4-ethylenedioxythiophene), poly (styrenesulfonic acid) (PEDOT: PSS). the photovoltaic effect was observed, characterized, and examined at a wavelength of 365 nm. ZnO NPs are coated with an indium tin oxide painted with glass at the top of the (PEDOT: PSS) layer. Then, aluminum is deposited on the top of the unit electrode. The current-voltage function exhibits the appropriate behavior in the dark field. With ultraviolet light, the backward orientation of current has been detected, as well as the forward orientation. Current-voltage data reveal that the barrier voltage drops down when exposed to UV light.

How to cite this article
Saeed A. A, Hussein A, Alaridhee T, and Malek F. Nanostructured PEDOT: PSS /ZnO Heterojunction Diodes as Ultraviolet Sensors. J Nanostruct, 2021; 11(3):446-455. DOI: 10.22052/JNS.2021.03.004

INTRODUCTION

In the last decade, global energy consumption and population have grown markedly, leading to the development of energy effective and reliable optical energy sensing devices [1-4]. Ultraviolet (UV) photodetectors (PDs) have currently attracted possible applications in culture, the scientific community, and military defense [5-7]. As reported in previous studies, the Ultraviolet (UV) photodetectors have been usually employed in different applications including safe space-to-space communications [8, 9], water sterilization [10], emissions control [11, 12], flaming sensing, and recently in the detection of missile plume [13], etc. The latter applications include devices with highly sensitive, strong signal to noise ratios and higher speeds in response [14]. A set of UV detectors exists such as Si-based photodetectors and photomultipliers. The features of these devices, involving low noise and fast response, allow a highly sensitive UV region. Nevertheless, these devices have some weaknesses, such as filters required to prevent low-energy photons (Vis-IR light), their damage and reduction in the performance (Si-based photodetectors), an extremely high vacuum atmosphere, and ultra-high voltage supply requirements [8]. Despite these limitations, the UV detectors have been acquiring great significance due to their wide visibility-dependent, small bandgap semi-conductor such as indium phosphide semiconductor. Furthermore, the materials having a wide bandgap are considered to be more stable in both chemically and thermally which is a benefit for devices operating in severe climates [15].

In the last few years, ZnO has been broadly demonstrated for its remarkable properties and

* *Corresponding Author Email: tahseen.alaridhee@uobasrah.edu.iq*

effective applications in optoelectronic systems [16, 17]. This material has high chemical stability, desirable radiation resistance, low cost, and a bandgap of 3.37 eV at room temperature [18, 19]. In the 1940s, Mollow first detected the UV radiation response in ZnO thin films [20]. However, since the 1980s, work on ZnO-based photodetectors has slowly evolved. In the beginning, the devices were simple in structure and their features were inconvenient. As reported by Fabricius H. in Ref. [21], many photodetectors based on ZnO were used by improving the manufacture of ZnO-based film in different methods. This has been seen in the case of the p-n junction, p-i-n junction, and Schottky junction, etc. Zinc Oxide is an inorganic semiconductor used as a UV sensor because of its UV absorption property [22]. The materials of ZnO NPs are presently employed as a layer for UV radiation detection in place of ZnO grain size [23-26]. Among the significant nanostructures, ZnO NPs are applied to sensors with a completely simple and cheap solution process. The manufacture of ZnO NPs thin films are less complicated than the atomizing method of making thin films. The ZnO NPs can also be combined with other semiconductors to optimize the electric performance of devices [27-30].

In polymers, the p-type semiconductor is also considered one of the materials that are widely used to design an electronic divider with ZnO nanostructure for use in UV sensors [31-33]. The p-type conductive organic materials are a good candidate for replacing or partnering with inorganic substances to reduce production costs [33-35]. Among all existing donor polymers and their derivatives, copolymers, analogs, the PEDOT: PSS (the abbreviation of poly(3,4-ethylenedioxythiophene)), is the best available PThs with regard to conductivity, stability, transparency, and biocompatibility. As a result of its inherent structural characteristics, excellent optical and electrical capabilities, and prospective applications, PEDOT has become a widely discussed and highly profitable subject for many scientific research groups [36-41]. PEDOT–PSS, a combination of positively charged conjugated PEDOT and negatively charged saturated PSS, has effectively addressed the solution-processability problem of electronic conducting polymers (ECPs) and developed into a commercially accessible aqueous dispersion of ECPs. Furthermore, PEDOT–PSSs, copolymers, analogs (PEDOT–PSSs), and even novel ECPs and their composites were created to overcome problems in academic and industry research and application. It has become apparent that the unique and multifaceted properties of PEDOT–PSS have been extensively studied to serve as a foundation for potential applications in the areas of organic/polymeric electronics and optoelectronics. In this paper, poly (styrene sulfonic acid) or PEDOT: PSS was used and ZnO NPs were prepared to produce a thin film layer on a thin film of PEDOT: PSS to design a hybrid divider by screen coating. Electron pairs-a gap resulting from the ZnO oxide layer's stimulation of ultraviolet radiation that is transmitted through this structure. Materials and sensors were marked out. UV responses were tested for UV detector applications in electrical conductors. The result obtained in this work is a contribution to confirm the efficiency of the blend of ZnO NPs and PEDOT: PSS.

MATERIALS AND METHODS

The indium tin oxide (ITO) coated glass substrate must be the etched process in the aluminum contacts area before materials deposition to avoid short circuits in the solar cell. To fabricate the p-type polymer, the PEDOT: PSS was used on the device. The latter is the form of an aqueous colloidal dispersion that was purchased from Sigma-Aldrich, Inc. which is composed of the PEDOT:PSS ratio as 1:2.5 (by weight), respectively. The dispersion is made up of submicrometer-sized gel particles that dry to produce a continuous conducting and transparent film. To prepare the PEDOT: PSS thin film, distilled water was used as a solvent for treating the PEDOT: PSS with 70/30 of sol concertation. The first step was polymer filtering by using Polytetrafluoroethylene (PTFE) membrane, pore Size (0.45µm). Thereafter, the resultant filtered PEDOT: PSS solutions were spin-coated on ITO glass substrates immediately. The spin coating method was used to deposit the PEDOT: PSS solution on top of the ITO surface at 2000 rpm for 30 s to form the first layer and dried by heating at 125 °C for 20 min to evaporate the solvent from the sample surface.

Zinc Oxide nanoparticles were prepared by using the sol-gel method. Solution has consisted of 0.5 M concentration of zinc acetate dihydrate [Zn $(CH_3COO)_2$. $2H_2O$] (Sigma–Aldrich, India) is placed in a 1.0 molar ratio of the mixture of absolute 2-methoxyethanol (Sigma–Aldrich, India) and

ethanolamine [$HOCH_2CH_2NH_2$] (Sigma–Aldrich, India). stirred at 60 °C for 1h. The resultant sol was heated under 60 °C for 1 h with constant stirring in order to get a clear and homogeneous solution. The precursor sol was kept at room temperature for 48 h to well complete the gelation and hydrolysis reaction. The deposition of ZnO thin film was prepared by cleaning the glass substrate with acetone and ethanol for 10 min in an ultrasonic cleaner. Thereafter, the samples were cleaned and rinsed in deionized water and heated in the oven at 110 °C for 20 minutes until being dried. The depositing of ZnO films was performed by using the spin-coating method. The spin coating procedure was carried out at 2000 rpm for 40 s. A hot plate in the air was used to dry the coated ZnO thin films at 200 °C for 15 minutes to eliminate the organic residual and evaporate the solvent as well. The processes from depositing to heating were repeated five times to get thin films with favorable thickness. To enhance the crystal structure of ZnO films, they were annealed at 350 °C for 2 hours to be used as n-type window layer and prepared for characterization. After the verification of ZnO thin film, the n-type ZnO was re-crystallized, and spin-coated (2000 rpm for 40 s) on the annealed PEDOT: PSS film. The thermal evaporation process is used to prepare a thin layer's electrodes of aluminum on top of the ZnO layer, each of which is (2 mm) wide. Therefore, for current-voltage measurements, two contacts were constructed, one from a thin ITO strip and the other from aluminum.

Fig. 1a shows a sensor connected to both points of measurement and controls of the UV lighting from the bottom of the sensor during the measuring process. Schematic Fig. 1b shows the top view of the sample. Each of the latter is made of two sensor cells and the operative electrode is the intersection between the sensor electrodes Al and ITO. The ZnO NPs and the structural analysis PEDOT: PSS/ZnO NPs thin films were characterized using a variety of techniques. The X-ray diffraction (Pert Pro MPD from Philips of the Netherlands) was used to characterize the structural properties of the ZnO and PEDOT: PSS/ ZnO coated films. The XRD pattern was produced by utilizing a Cu-K radiation source with (λ= 1.5406 nm) as an X-ray diffractometer at 40 kV and 30 mA. The scan rate and step size are 20 minutes, and 0.018°, respectively. The optical properties of the samples were studied using a double beam UV/VIS spectrophotometer (Shimadzu UV-160A) within 300-900 wavelength. The energy gap E_g of these films can be determined by the relation between the coefficient of absorption and the energy of the photons. Scanning Electron Microscope (SEM) was used to determine the morphological characteristics of ZnO NPs and PEDOT/ZnO, thin films, particularly their size and form (Leo-Supra 50VP (Carl Zeiss, Germany)). The UV sensor's current-voltage curve (I-V) properties were measured using Keithley 4200-SCS in measurement units (SMUs). An electrical response was detected through changing the device resistance in UV illumination and dark field at 365 nm of the UV light sensors. The current and resistance were estimated by using two scales of Keithley SMUs and LCR (GW Instek LCR-819), respectively.

RESULTS AND DISCUSSIONS

The surface analysis of both ZnO NPs and PEDOT: PSS: ZnO NPs thin films were investigated by Scanning Electron Microscopy (SEM). The SEM

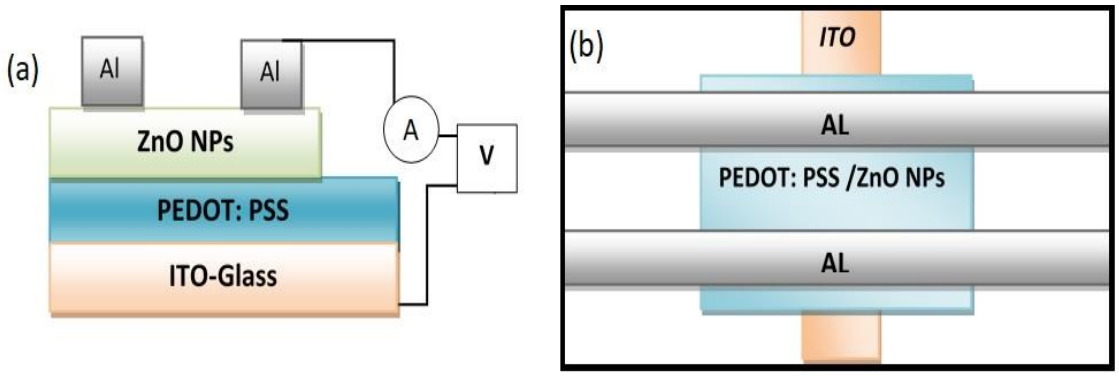

Fig. 1. (a) Schema showing the UV sensor structures the side view; (b) and the top view.

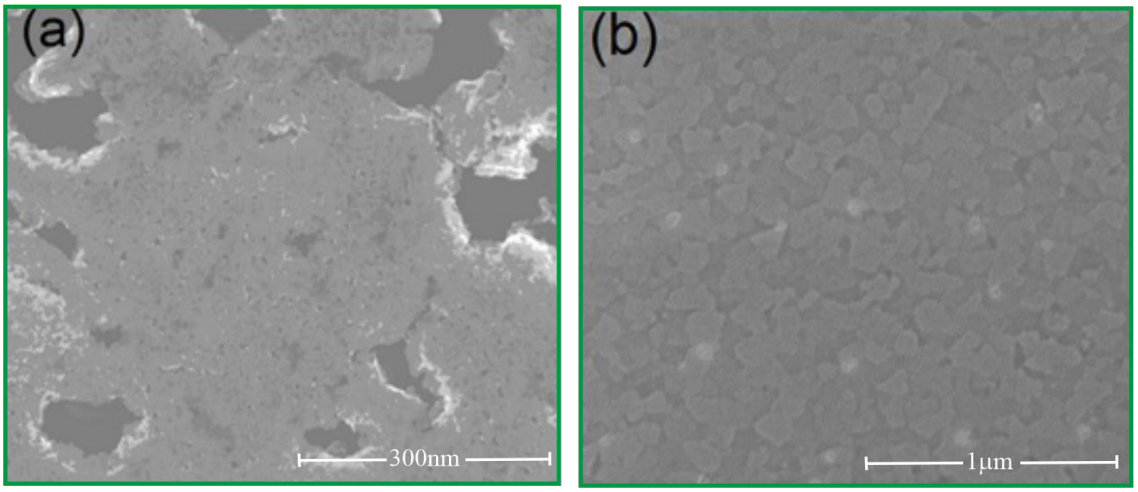

Fig. 2. (a) SEM images of ZnO NPs; (b) and PEDOT: PSS: ZnO NPs thin films.

micrographs of the samples were magnified by 60 Kx and 200 Kx times. The surface morphology, presented in Fig. 2a of the prepared ZnO NPs taken for a selected position of the film, shows the aggregation of tiny particles.

Samples were magnified by 60 Kx and 200 Kx times. In Fig. 2b, it can be observed a rough surface of uniformly distributed flake-like grains due to the addition of the PEDOT: PSS layer and the aggregate ZnO NPs, which will increase the roughness surface further.

To verify the presence of PEDOT/ZnO NPs, the samples were examined by X-ray diffraction pattern (XRD). Fig. 3 shows the X-ray diffractogram of crystallite size of ZnO NPs, where the reflections of planes (100), (002), (101), (102), (110), and (103) correspond to the ZnO wurtzite structure (JCPDS Data Card No:036-1451) and

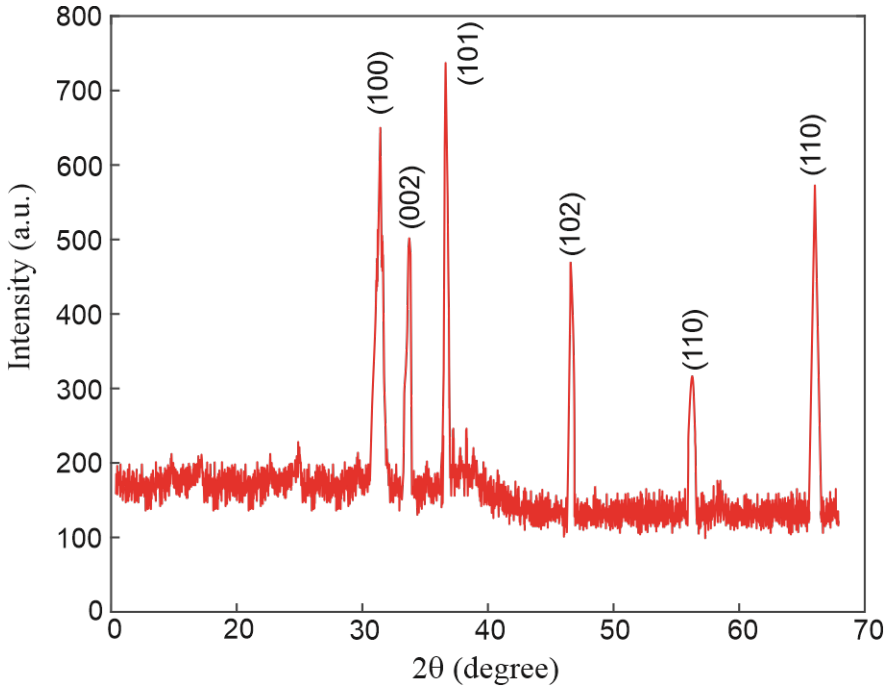

Fig. 3. XRD pattern of PEDOT: PSS/ZnO nanoparticles synthesized.

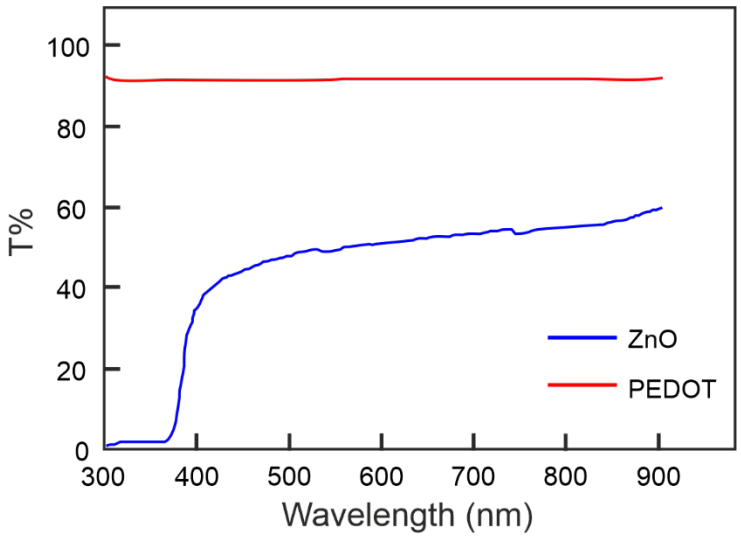

Fig. 4. Optical transmission via ZnO NPs and PEDOT: PSS thin films.

corresponding to peaks at 31.3°, 33.7°, 36.65°, 46.36°, 56.46°, and 63.14° respectively [42]. The Debye-Scherrer formula was used to determine the average particle size of the ZnO thin film based on XRD measurements [43]. By using this relation below, the crystallite grain size D for ZnO NP can be calculated as follow:

$$D = {0.9\,\lambda}/{\beta\cos\theta} \quad (1)$$

Where λ is the wavelength of X-ray (1.5406 nm), β represents the diffraction line broadening estimated at half of its maximum intensity in radians, and θ is the diffraction angle. The

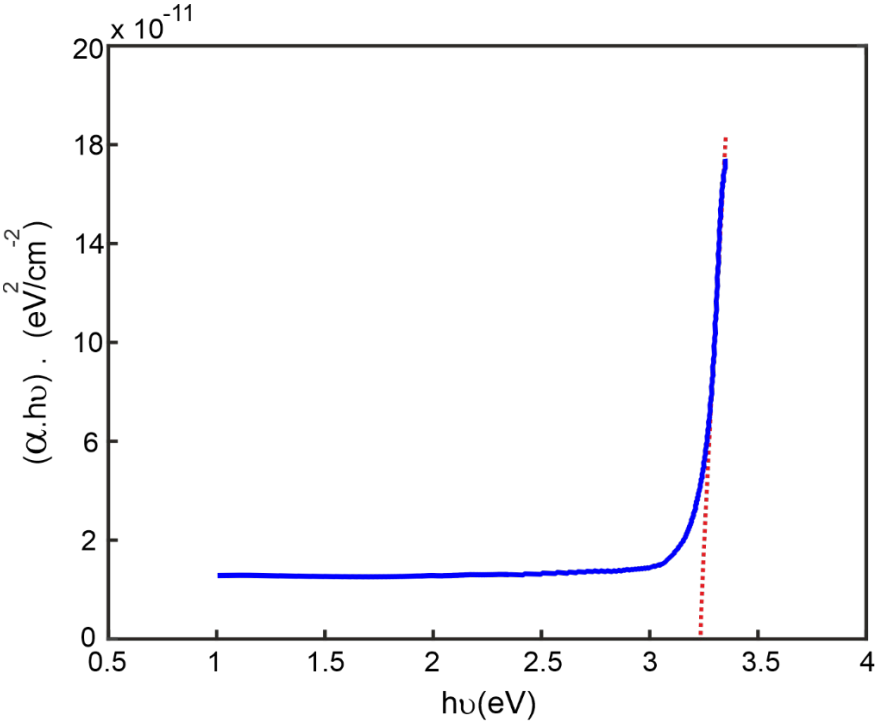

Fig. 5. The calculated energy gap of ZnO thin film versus the photon energy.

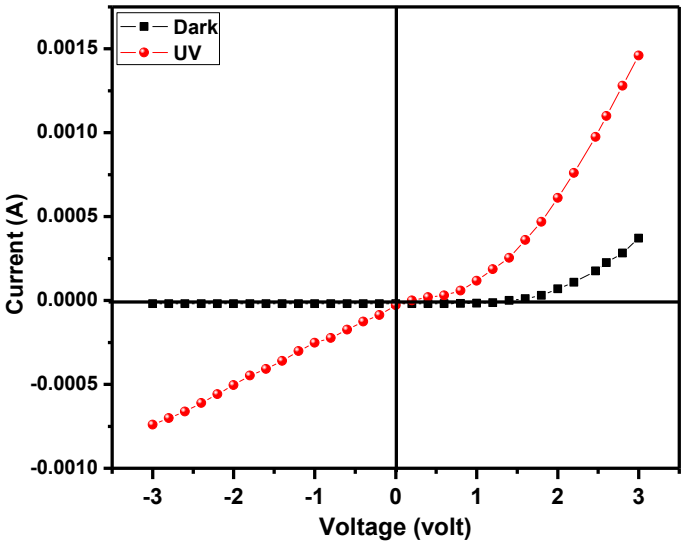

Fig. 6. I-V Sensor characteristics in darkfield and UV exposure.

crystallite grain size of ZnO particles was found approximately 6 nm. As can see in Fig. (3), the intensity is about thirty times higher than the intensity of PEDOT polymer. This interpretation is based on the amorphous structure achieved by the invisible peaks of the PEDOT: PSS sample.

Optical properties

The UV-Vis spectrometer was used to measure the optical transmission of thin film and compared to a reference as Pure PEDOT: PSS thin film in measurement. The PEDOT: PSS films have transmission spectra curves quite smooth and had a uniformly flat surface after the annealing process (see Fig. 4). The Transmittance of PEDOT: PSS layer is very high (i.e., absorption very low). Transmittance is ~ 95% in the visible range for PEDOT: PSS layer. According to the results, the high transparency character of PEDOT: PSS thin was observed in the UV to NIR band. On the other hand, the optical energy gap of ZnO NPs is predicted from the efficiency of the absorption edge which is located at~ 370 nm in the transmission spectrum [24, 27]. It is worth that the absorption edge of ZnO NPs thin film on the optical absorption UV band could not affect by PEDOT: PSS blend. This latter result ensures that the ZnO NPs thin film is a promising candidate to design UV sensors operating in several applications.

In the absorption region, the estimation of the absorption coefficient α becomes necessary in identifying the changes in the electronic structure of ZnO NPs thin film. The factor α can be calculated from the expression below:

$$\alpha = \frac{1}{d}\ln\left[\frac{(1-R)^2}{2T} + \sqrt{\frac{(1-R)^4}{4T^2} + R^2}\right] \quad (2)$$

where R and T are the reflection and transmittance, respectively, and d represents the thickness of the thin film. The latter is estimated via the classical method that requires the spectroscopic ellipsometry (SE) device (M2000V, J.A. Wollma Co., Inc.) working in the wavelength range 350 nm to 900 nm. The obtained values for both ZnO and PEDOT: PSS thin film under study were 40 nm and 64 nm, respectively. The estimated factor α is frequently used to classifying the optical energy gap, also known as the absorption edge. The intercept of $(ahu)^m$ versus hu with the x-axis was used to get the energy bandgap values in this investigation, (i.e. $(ahu)^m = 0$) (see Fig. 5). This latter is produced from Tauc's equation, which is given by [43]:

$$\alpha h\upsilon = A\left(h\upsilon - E_g\right)^m \quad (3)$$

Where A is a transition probability-dependent constant, E and E_g represent the photon energy and the optical energy gap, respectively. The factor g represents the distribution of the density of states index, which is based on transition type (indirect is 2 and 3 for allowed and direct is 1/2

and 3/2 for allowed and forbidden, respectively). As depicted in

Fig. 5, and by substituting for index m with 2 (see Eq. 3), one can deduce the optical energy gap which equals 3.2 eV. The value of m is adopted as a result of the factor a is less than 10^4 (depending on Eq. 2), which denotes that the transition between energy states was direct. The value of E_g obtained in Fig. 5 is in agreement with the energy bandgap of ZnO NPs.

Electrical Properties

Fig. 6 shows the current-voltage (I -V) characteristics of ITO/PEDOT: PSS/ZnO NPs/Al at dark field and UV radiation configuration. As seen in Fig. 6, the heterojunction exhibits an evolution at the interlayer PEDOT: PSS and ZnO NPs. In addition, the I-V relation in the dark field displays rectifier-like or diode behavior. The characteristic of the sensor used, in this work, has only forward bias. Therefore, the current cannot be transferred via a device with reverse bias or applied negative voltage. On the other hand, the current with backward and forward bias voltage increases in UV radiation. This produced current is greater than in the dark field, as the potential barrier at the heterojunction decreases. The diode-like behavior of the PEDOT: PSS/ZnO NPs heterojunction was demonstrated with the thermal radiation concept. The latter is applied to estimate the data to determine the variation in potential barrier height [44, 45]. The link between the current and the forward bias can be written as follows:

$$I = I_s\left[\exp\left(\frac{qV}{nK_BT}\right) - 1\right] \quad (4)$$

Where I_s represents the saturation current, q is the elementary charge, V represents the applied

forward voltage, n is the ideality factor, K_B represents the Boltzmann constant and T is the absolute temperature. The saturation current I_s can express as:

$$I_s = AA^*T^2\exp\left(\frac{-q\phi_B}{K_BT}\right) \quad (5)$$

Where A and A* Represent the junction area and the appropriate constant of Richardson, respectively, and φ_B the potential height of the barrier at the ZnO / PEDOT: PSS interface. The A* of ZnO takes the value of ~ 36 $Acm^{-2}K^{-2}$ [39, 46], and for this case, the effective sensor junction area is 2×10^{-2} cm^2.

In Fig. 7a & b, the plot of semilogarithmic for I / [1- exp (-qV/K_B T)] versus voltage (i.e., forward bias) of the sensor in both darkfield and UV illumination. The values of the barrier height φ_B and ideal factor n can obtain by employing a linear fitting slope and intercept in the lower power region. The sensor ideality factors ~2.6 for the dark and ~2.9 for UV lighting. The Sah-Noyce-Shockley model expects ideal factors at low voltage and high voltage, 1 and 2, respectively. The higher n value achieved in our sensor junction indicates that PEDOT's behavior: PSS/ZnO NPs junction diode deviates from ideal performance. This can be because surface states are existent in ZnO NPs. The current or charging path may also increase due to an increase in energy levels on the surface [33, 37]. These surface states offer additional energy states that are responsible for multiple current pathways that yield a higher value of the ideal factor.

Constructively, the obtained findings of barrier

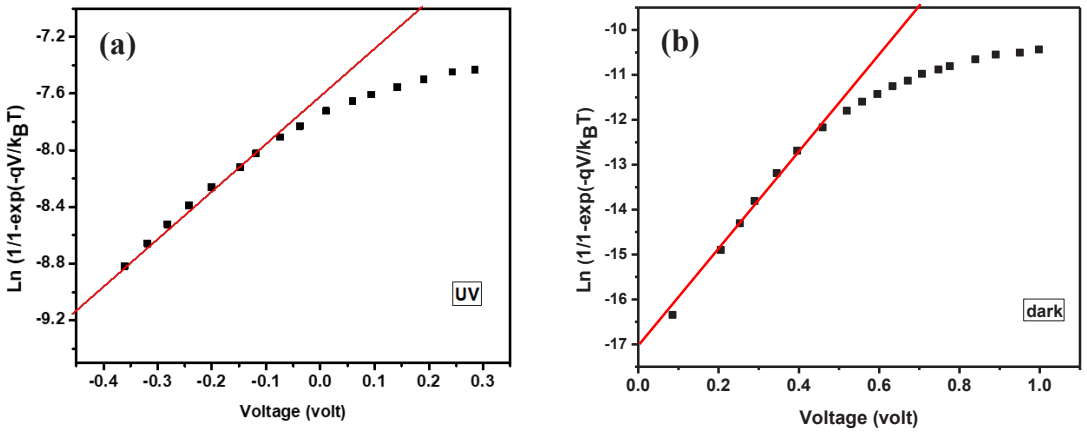

Fig. 7. Current in a logarithmic scale of (a) dark field and (b) UV light versus system voltage.

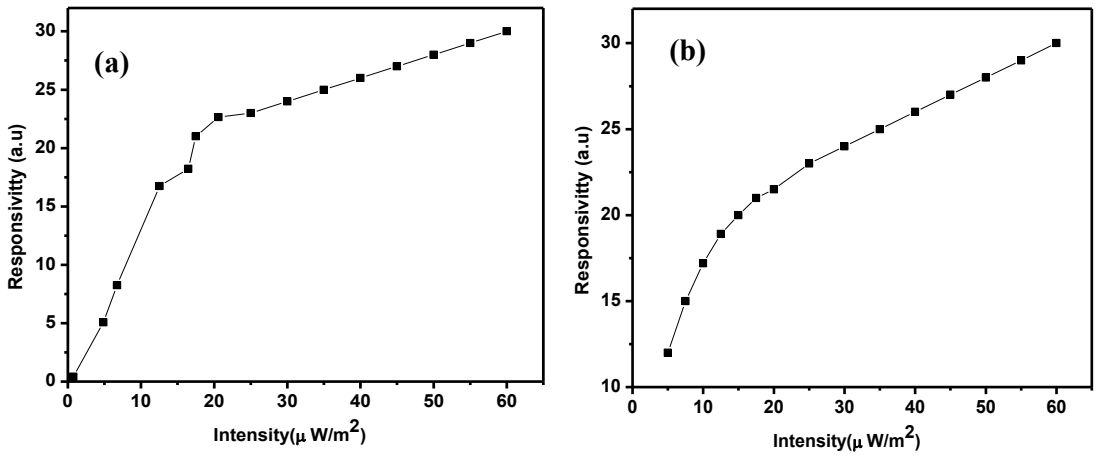

Fig. 8. UV light sensor response versus their intensities with PEDOT: PSS/ZnO NPs heterojunction nanostructure at wavelength of (a) 360 nm and (b) 365 nm.

height φ_B are approximately 0.78 eV and 0.63 eV for the dark field and the UV illumination, respectively. It is clear that φ_B decreases as the sensor is irradiated by UV light. This latter behavior is according to the energy band structure at the connection between PEDOT: PSS and hence the ZnO NPs can modify through decreasing the potential barrier, whereas the produced carriers present an increase in the ZnO NPs layer. Consequently, stimulation resulted from UV illumination leads to the current be transported through heterojunction.

Fig. 8a depicted that the UV response of the sensor versus the intensity. The optical response is estimated by finding the resistance difference of the sensor concerning the darkfield, the illumination wavelength (l~360 nm), and intensity. At the band spectra ranging

between 300 to 390 nm, the sensor exhibits a significant response at its absorption band of ZnO NPs. As shown in Fig. 8b, when the distance between the UV source and sensor is varied, the latter presents a response to UV irradiation at a distinct value of intensity.

The sensor response intensity of the optical radiation of UV light displays evolution in power function law relationship [47, 48]. The sensor response magnifies when the UV light intensity increases and tends to be saturated at a value greater than 20 μW/cm^2. The significant electrical signal at varying UV light intensity leads to the possibility of applying for electronic circuits having a UV detector system to fix the level of UV light in such areas.

CONCLUSIONS

The solution-based UV light sensor with the heterojunctions between PEDOT: PSS and ZnO NPs clearly showed the electric response under Ultraviolet radiation. Changes in current and sensor resistance were examined in the UV response. The potential electronic interconnection barrier height can be produced from the current-voltage characteristic with a reduction in UV lighting. Therefore, higher device conductivity is obtained below 365 nm UV exposure. The UV sensor can show the UV intensity level. This work also offers an incentive to further optimize sensor electrical response for UV operating systems.

ACKNOWLEDGMENTS

The authors would like to thank Mustansiriyah University and Polymer Research Center (PRC), University of Basrah, for their support in this work.

CONFLICT OF INTEREST

The authors declare that there is no conflict of interests regarding the publication of this manuscript.

REFERENCES

1. Teng F, Hu K, Ouyang W, Fang X. Photoelectric Detectors Based on Inorganic p-Type Semiconductor Materials. Adv Mater. 2018;30(35):1706262.
2. Bhandari S, Mondal D, Nataraj SK, Balakrishna RG. Biomolecule-derived quantum dots for sustainable optoelectronics. Nanoscale Advances. 2019;1(3):913-936.
3. Ouyang W, Teng F, He J-H, Fang X. Enhancing the Photoelectric Performance of Photodetectors Based on Metal Oxide Semiconductors by Charge-Carrier Engineering. Adv Funct Mater. 2019;29(9):1807672.

4. Chen H, Su L, Jiang M, Fang X. Highly Desirable Photodetectors Derived from Versatile Plasmonic Nanostructures. Adv Funct Mater. 2017;27(45):1704181.
5. Zhou J, Chen L, Wang Y, He Y, Pan X, Xie E. An overview on emerging photoelectrochemical self-powered ultraviolet photodetectors. Nanoscale. 2016;8(1):50-73.
6. Zhang Y, Xu W, Xu X, Cai J, Yang W, Fang X. Self-Powered Dual-Color UV–Green Photodetectors Based on SnO2 Millimeter Wire and Microwires/CsPbBr3 Particle Heterojunctions. The Journal of Physical Chemistry Letters. 2019;10(4):836-841.
7. Tong T, Wang S, Zhao J, Cheng B, Xiao Y, Lei S. Erasable memory properties of spectral selectivity modulated by temperature and bias in an individual CdS nanobelt-based photodetector. Nanoscale Horizons. 2019;4(1):138-147.
8. Muñoz E, Monroy E, Pau JL, Calle F, Omnès F, Gibart P. III nitrides and UV detection. J Phys: Condens Matter. 2001;13(32):7115-7137.
9. Xie Y, Wei L, Wei G, Li Q, Wang D, Chen Y, et al. A self-powered UV photodetector based on TiO2 nanorod arrays. Nanoscale research letters. 2013;8(1):188-188.
10. Al-Shamma'a AI, Pandithas I, Lucas J. Low-pressure microwave plasma ultraviolet lamp for water purification and ozone applications. J Phys D: Appl Phys. 2001;34(18):2775-2781.
11. Obertacke R, Wintrich H, Wintrich F, Leipertz A. A New Sensor System for Industrial Combustion Monitoring and Control using UV Emission Spectroscopy and Tomography. Combustion Science and Technology. 1996;121(1-6):133-151.
12. Huang T-Y, Chen C-H, Lin C-C, Lee Y-J, Liu C-L, Liou G-S. UV-sensing organic phototransistor memory devices with a doped organic polymer electret composed of triphenylamine-based aggregation-induced emission luminogens. Journal of Materials Chemistry C. 2019;7(35):11014-11021.
13. Monroy E, Calle F, Pau JL, Muñoz E, Omnès F, Beaumont B, et al. AlGaN-based UV photodetectors. Journal of Crystal Growth. 2001;230(3-4):537-543.
14. Sun J, Zhan T, Liu Z, Wang J, Yi X, Sarro PM, et al. Suspended tungsten trioxide (WO3) gate AlGaN/GaN heterostructure deep ultraviolet detectors with integrated micro-heater. Optics Express. 2019;27(25):36405.
15. R A, R R, R L, Vavilapalli DS, Baskar K, Singh S. Large area ultraviolet photodetector on surface modified Si:GaN layers. Applied Surface Science. 2018;435:1057-1064.
16. Özgür Ü, Alivov YI, Liu C, Teke A, Reshchikov MA, Doğan S, et al. A comprehensive review of ZnO materials and devices. Journal of Applied Physics. 2005;98(4):041301.
17. Ferhati H, Djeffal F, Benhaya A, Martin N. Highly sensitive, ultra-low dark current, self-powered solar-blind ultraviolet photodetector based on ZnO thin-film with an engineered rear metallic layer. Mater Sci Semicond Process. 2020;110:104957.
18. Arora A, Devi S, Jaswal V, Singh J, Kinger M, Gupta V. Synthesis and characterization of ZnO nanoparticles. Oriental Journal of Chemistry. 2014;30(4):1671-1679.
19. Harun K, Mansor N, Ahmad ZA, Mohamad AA. Electronic Properties of ZnO Nanoparticles Synthesized by Sol-gel Method: A LDA+U Calculation and Experimental Study. Procedia Chemistry. 2016;19:125-132.
20. Matossi F. Photoconductivity Conference . Held at Atlantic City, 4-6 Nov. 1954. Sponsored by the University of Pennsylvania, Radio Corporation of America, and Office of Naval Research. R. G. Breckenridge, chairman, Editorial Committee. Wiley, New York; Chapman and Hall, London, 1956. 653 pp. Illus. $13.50. Science. 1957;125(3246):505-505.
21. Fabricius H, Skettrup T, Bisgaard P. Ultraviolet detectors in thin sputtered ZnO films. Applied Optics. 1986;25(16):2764.
22. Brillson L, Cox J, Gao H, Foster G, Ruane W, Jarjour A, et al. Native Point Defect Measurement and Manipulation in ZnO Nanostructures. Materials (Basel, Switzerland). 2019;12(14):2242.
23. Huang H-Y, Chiang H-J, Wu C-Z, Lin Y, Shen Y-K. Analysis on Characteristics of ZnO Surface Acoustic Wave with and without Micro-Structures. Micromachines. 2019;10(7):434.
24. Ghosh SP, Das KC, Tripathy N, Bose G, Kim DH, Lee TI, et al. Ultraviolet photodetection characteristics of Zinc oxide thin films and nanostructures. IOP Conference Series: Materials Science and Engineering. 2016;115:012035.
25. Li H-G, Wu G, Chen H-Z, Wang M. Polymer/ZnO hybrid materials for near-UV sensors with wavelength selective response. Sensors Actuators B: Chem. 2011;160(1):1136-1140.
26. Zheng M, Gui P, Wang X, Zhang G, Wan J, Zhang H, et al. ZnO ultraviolet photodetectors with an extremely high detectivity and short response time. Applied Surface Science. 2019;481:437-442.
27. Semaltianos NG, Logothetidis S, Hastas N, Perrie W, Romani S, Potter RJ, et al. Modification of the electrical properties of PEDOT:PSS by the incorporation of ZnO nanoparticles synthesized by laser ablation. Chemical Physics Letters. 2010;484(4-6):283-289.
28. G H, Vempati S, Prajapati KN, Bandopadhyay K, Kalathingal V, Mitra J. Negative photoresponse in ZnO–PEDOT:PSS nanocomposites and photogating effects. Nanoscale Advances. 2019;1(6):2435-2443.
29. Chang H, Sun Z, Ho KY-F, Tao X, Yan F, Kwok W-M, et al. A highly sensitive ultraviolet sensor based on a facile in situ solution-grown ZnO nanorod/graphene heterostructure. Nanoscale. 2011;3(1):258-264.
30. Fouda AN, El Basaty AB, Eid EA. Photo-Response of Functionalized Self-Assembled Graphene Oxide on Zinc Oxide Heterostructure to UV Illumination. Nanoscale research letters. 2016;11(1):13-13.
31. Belhaj M, Dridi C, Yatskiv R, Grym J. The improvement of UV photodetection based on polymer/ZnO nanorod heterojunctions. Org Electron. 2020;77:105545.
32. Wu W, Bian JM, Sun JC, Cheng CH, Wang YX, Luo YM. A comparative study of ZnO film and nanorods for ZnO/polyfluorene inorganic/organic hybrid junction. Journal of Alloys and Compounds. 2012;534:1-5.
33. Hussein AA, Saeed AA, Alaridhee TA, Malek FH. Enhancement efficiency of poly (o-toluidine) ZnO solar cells by using metal oxide-assisted poly (styrenesulfonate) poly (o-toluidine) poly (3,4ethylenedioxythiophene) nanostructures. 2ND INTERNATIONAL CONFERENCE ON MATERIALS ENGINEERING & SCIENCE (IConMEAS 2019): AIP Publishing; 2020.
34. Adhikari B, Majumdar S. Polymers in sensor applications. Prog Polym Sci. 2004;29(7):699-766.
35. Boroomand Nasab B, Kosarian A, Sheini NA. Effect of Oxygen Flow Rate in Zinc Oxide Radio Frequency Magnetron Sputtering on the Structural and Optical Properties of ZnO|PEDOT:PSS Inorganic|Organic Hetero-Junction. Semic.

2020;54(8):844-852.
36. Elschner A, Kirchmeyer S, Lovenich W, Merker U, Reuter K. PEDOT: CRC Press; 2010 2010/11/02.
37. Groenendaal L, Jonas F, Freitag D, Pielartzik H, Reynolds JR. Poly(3,4-ethylenedioxythiophene) and Its Derivatives: Past, Present, and Future. Adv Mater. 2000;12(7):481-494.
38. Kirchmeyer S, Reuter K. Scientific importance, properties and growing applications of poly(3,4-ethylenedioxythiophene). Journal of Materials Chemistry. 2005;15(21):2077.
39. Martin DC, Wu J, Shaw CM, King Z, Spanninga SA, Richardson-Burns S, et al. The Morphology of Poly(3,4-Ethylenedioxythiophene). Polymer Reviews. 2010;50(3):340-384.
40. Wei W, Wang H, Hu YH. A review on PEDOT-based counter electrodes for dye-sensitized solar cells. IJER. 2014;38(9):1099-1111.
41. Rozlosnik N. New directions in medical biosensors employing poly(3,4-ethylenedioxy thiophene) derivative-based electrodes. Analytical and Bioanalytical Chemistry. 2009;395(3):637-645.
42. The Concepts of Intelligent Macromolecules and Smart Devices. Engineering Materials and Processes: Springer-Verlag. p. 1-37.
43. Brewster, Ray Q. Organic chemistry. New York: Prentice-Hall, Inc., 1953. 855 P. $7.00. SciEd. 1954;38(4):320-320.
44. Soylu M, Girtan M, Yakuphanoglu F. Properties of PEDOT:PEG/ZnO/p-Si heterojunction diode. Materials Science and Engineering: B. 2012;177(11):785-790.
45. Abdel-Khalek H, El-Samahi MI, El Salam MA, El-Mahalawy AM. Fabrication and performance evaluation of ultraviolet photodetector based on organic /inorganic heterojunction. CAP. 2018;18(12):1496-1506.
46. Sharma BK, Khare N, Ahmad S. A ZnO/PEDOT:PSS based inorganic/organic hetrojunction. Solid State Communications. 2009;149(19-20):771-774.
47. Chen H, Hu L, Fang X, Wu L. General Fabrication of Monolayer SnO2 Nanonets for High-Performance Ultraviolet Photodetectors. Adv Funct Mater. 2012;22(6):1229-1235.
48. Yan J, Chen Y, Wang X, Fu Y, Wang J, Sun J, et al. High-performance solar-blind SnO2 nanowire photodetectors assembled using optical tweezers. Nanoscale. 2019;11(5):2162-2169.